Max-Planck-Institut
für Mathematik
in den Naturwissenschaften
Leipzig

Soft elastic response of stretched sheets of nematic elastomers: a numerical study

by

S. Conti, A. DeSimone and G. Dolzmann

SOFT ELASTIC RESPONSE OF STRETCHED SHEETS OF NEMATIC ELASTOMERS: A NUMERICAL STUDY

S. CONTI, A. DESIMONE, AND G. DOLZMANN

ABSTRACT. Stretching experiments on sheets of nematic elastomers have revealed soft deformation modes and formation of microstructure in parts of the sample. Both phenomena are manifestations of the existence of a symmetry-breaking phase transformation from a random, isotropic phase to an aligned, nematic phase. The microscopic energy proposed by Bladon, Terentjev and Warner [Phys. Rev. E 47 (1993), 3838] to model this transition delivers a continuum of symmetry-related zero-energy states, which can be combined in different ways to achieve a variety of zero-energy macroscopic deformations.

We replace the microscopic energy with a macroscopic effective energy, the so-called quasiconvexification. This procedure yields a coarse-grained description of the physics of the system, with (energetically optimal) small-scale oscillations of the state variables correctly accounted for in the energetics, but averaged out in the kinematics. Knowledge of the quasiconvexified energy enables us to compute efficiently with finite elements, and to simulate numerically stretching experiments on sheets of nematic elastomers.

Our numerical experiments show that up to a critical, geometry-dependent stretch, no reaction force arises. At larger stretches, a force is transmitted through parts of the sheet and, although fine phase mixtures disappear from most of the sample, microstructures survive in some pockets. We reconstruct from the computed deformation gradients a possible composition of the microstructure, thereby resolving the local orientation of the nematic director.

1. INTRODUCTION

The elastic properties of weakly cross-linked nematic chains display in an experimentally accessible setting the fascinating consequences of non-uniqueness of energy-minimizing states. As first predicted by Golubović and Lubensky (1989), isotropic gels prepared by cross-linking liquid polymers with a nearby nematic phase are, at least in some cases, close to a transition to an anisotropic phase, characterized by the coupling of elastic deformations to the alignment of the nematic director (see Figure 1). The elastic energy is then approximately minimized by all volume-preserving uniaxial deformations of given magnitude, independently of the orientation of the principal stretch directions (Bladon et al., 1993; Verwey et al., 1996; Warner and Terentjev, 1996). These states form the zero set of the so-called microscopic energy W. Furthermore, all states with smaller stretches can be obtained by combining zero-energy states with different orientations in different parts of the domain, i.e., by using suitable mixtures of pure states (obtaining the so-called stripe-domain states, see Verwey et al., 1996). In a loading experiment where uniaxial affine deformations are imposed one expects a window of strains for which

the stress is essentially zero ("liquid phase"), and a standard rubber-like response ("solid phase") for strains larger than the critical one corresponding to the pure phase aligned with the externally imposed stretch. These deformation processes are accompanied by a reorientation of the nematic director which, in the final pure phase, is aligned with the external stretch.

Experimental measurements on nematic elastomers, starting from the work of Kundler and Finkelmann (1995), have been understood by studying affine deformations within the general picture described above, even though the need for refinements in various directions has clearly emerged. For example, detailed measurements of the elastic response have shown that the "liquid" phase can actually sustain small stresses, and this has been explained by additional effects, such as residual nematic order at high temperatures, polydomains, fluctuations in chemical composition (Warner, 1999), or competition of the bulk energy with a gradient energy of Oseen-Frank-type which penalizes spatial oscillations of the nematic director (Weilepp and Brand, 1996; Finkelmann et al., 1997). Typical experimental measurements are made by stretching clamped thin sheets. The presence of the clamps induces nonuniform stretches in the sample, but the effects of spatial stress inhomogeneity have been up to now neglected. Analogously, the observation of microstructure formation only in some parts of the sample (Zubarev et al., 1999) is not explained by an analysis restricted to affine deformations.

The goal of this paper is to carefully study the predictions of the general theory in realistic loading geometries, including quantitative estimates of the inhomogeneous stress distribution, which are naturally computed with finite-element numerics. We adopt the model energy of Bladon et al. (1993), which neglects higher order gradients, composition inhomogeneities and all effects responsible for the small-stress threshold. This energy has no intrinsic length scale, hence it is unable to establish a finite size for the oscillations of the nematic director. Thus, we choose to work with an ideally soft system, and we do not attempt to resolve numerically the geometry of the microstructures arising from the non-convexity of W. Instead, we use a "coarse-grained" version of the microscopic energy W, its quasiconvex envelope W_{qc}. This means that energetically optimal small-scale oscillations are correctly accounted for in the energetics, but averaged out in the kinematics. Numerical computations based on W_{qc} need then only to resolve the macroscopic length scales associated with spatial variations of the internal stresses, not the finer (in this approximation, potentially infinitesimal) length scales of the local oscillations.

The relevance of the coarse-grained energy W_{qc} is not limited to its positive impact on computations: the analytic expression of W_{qc} leads to the discovery of a surprising new feature in the mechanical behavior of nematic elastomers. Indeed, the macroscopic energy W_{qc} exhibits three distinct regimes, corresponding to three different response modes of the underlying fine phase mixtures. Besides a liquid-like and a rubber-like solid response, both of which had been discussed extensively in the previous literature, a smectic-like phase has emerged from our analysis. When the material is strongly compressed, say, along a direction $\mathbf{e}$, it reacts elastically to stretches along $\mathbf{e}$, but there exist shears in the plane orthogonal to $\mathbf{e}$ against which the response is completely soft. We find that this newly discovered phase plays a crucial role in the mechanism of stress transmission within a stretched sheet, and we conjecture that some of the spatially inhomogeneous microstructures reported by Zubarev et al. (1999) should be composed of this smectic-like phase.
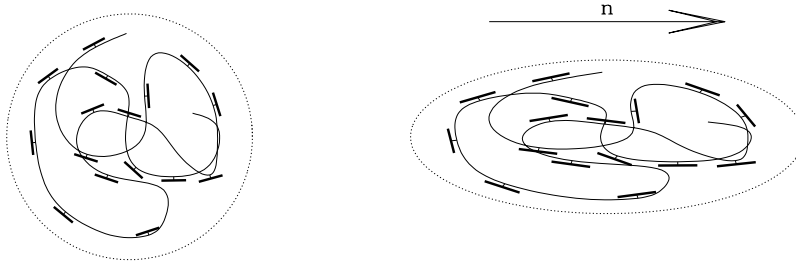
FIGURE 1. Schematic representation of the deformation mechanism associated with the isotropic-nematic transition. In the isotropic phase (left panel) the polymer can be imagined as a Gaussian coil with attached side mesogens, whose orientation is random. In the nematic phase (right panel) the mesogens have a tendency to align, and this induces a uniaxial deformation of the coil.

Based on the implementation of the quasiconvex energy W_{qc} in a finite-element code, we perform the first study of non-affine deformations of sheets of nematic elastomers, in a geometry that reproduces the clamped stretching experiments of Kundler and Finkelmann (1995) and following papers. We show that the liquid-like response at small stretch survives the change from homogeneous to non-homogeneous states of deformation, but the range of stretches in which it may occur is reduced with respect to the homogeneous case, by an amount depending on the aspect ratio of the sample. At stretches higher than the liquid threshold, we observe that only states with smectic microstructure survive, and that they are confined to two pockets close to the clamps. Transmission of stress occurs along an X-shaped path connecting the center of the sample to the endpoints of the clamps. Some sharp kinks in the stress transmission path emerge as a characteristic mark of the newly discovered smectic-like phase. Finally, we reconstruct the orientation of the nematic director from the computed deformation gradients, and compare our numerical results with existing experimental observations.

This paper is organized as follows. In Section 2 we briefly review the literature on the origin and the significance of the microscopic energy W and its effective counterpart W_{qc}. In Section 3 we present our computations and illustrate their implications. Finally in Section 4 we discuss methodological aspects and give some technical details on our computations.

2. THE MICROSCOPIC MODEL AND ITS EFFECTIVE MACROSCOPIC COUNTERPART

The fascinating material instabilities displayed by nematic elastomers are easily understandable as a consequence of the symmetry-breaking phase transition which establishes the orientational order of the nematic phase. We briefly summarize the heuristic derivation of the microscopic energy (4) in a simple case, referring to the literature (Bladon et al., 1993; Verwey et al., 1996; Warner and Terentjev, 1996;

Warner, 1999) for a more detailed analysis, which includes some information on the cross-linking process.

Nematic elastomers are polymeric chains that have nematic mesogens (i.e. rigid rod-like molecules) attached sideways to the polymeric backbone. At high temperature, the mesogens are randomly oriented, and the polymeric chains are spherical random coils. Below the isotropic to nematic transition temperature T_c the nematic mesogens align in some direction $\mathbf{n}$, called the director, and the polymer chains distort. The distortion is such that the chains are elongated in the direction $\mathbf{n}$, and this results in a volume-preserving uniaxial stretch of the whole network along $\mathbf{n}$ (as shown schematically in Figure 1), described by

$$(1) \qquad U_{\mathbf{n}} = a^{-1/3}\, \mathbf{n} \otimes \mathbf{n} + a^{1/6}(\mathrm{Id}_3 - \mathbf{n} \otimes \mathbf{n})\,.$$

Here, $a < 1$ is a material parameter which determines the magnitude of the stretch, Id_3 is the 3×3 identity matrix, and $(\mathbf{n} \otimes \mathbf{n})_{ij} = n_i n_j$. The reason for this definition of a will become clear after Eq. (4). For example, a unit ball is mapped by $U_{\mathbf{n}}$ into a prolate spheroid, with major axis of length $a^{-1/3}$ along $\mathbf{n}$, and minor axes of length $a^{1/6}$. The resulting set of natural states, i.e., of preferred stress-free states of distortion, is

$$(2) \qquad \mathcal{K} = \bigcup_{|\mathbf{n}|=1} SO(3)U_{\mathbf{n}}$$

where $SO(3)$ is the group of rotations. The set $\mathcal{K}$ can be equivalently characterized as the set of 3×3 matrices whose singular values are $(a^{1/6}, a^{1/6}, a^{-1/3})$,

$$(3) \qquad \mathcal{K} = \left\{ Q \begin{pmatrix} a^{1/6} & 0 & 0 \\ 0 & a^{1/6} & 0 \\ 0 & 0 & a^{-1/3} \end{pmatrix} Q', \quad Q, Q' \in SO(3) \right\}\,.$$

The free energy of this system was computed, in the Gaussian approximation, by Bladon et al. (1993). This energy can be heuristically understood as the appropriate measure of the distance of a given deformation gradient from the set $\mathcal{K}$. As in our earlier papers (DeSimone, 1999; DeSimone and Dolzmann, 2000), we take as reference configuration the stress-free state of the isotropic high-temperature phase instead of using the nematic phase in which the cross-linking was done. This amounts to an affine change of variables, which transforms the expression of Bladon, Terentjev, and Warner into

$$(4) \qquad W(F) = \begin{cases} \lambda_1^2(F) + \lambda_2^2(F) + a\lambda_3^2(F) - 3a^{1/3} & \text{if } \det F = 1 \\ +\infty & \text{else} \end{cases}$$

where $\lambda_1(F) \leq \lambda_2(F) \leq \lambda_3(F)$ are the ordered singular values of the deformation gradient $F = \nabla y$, y being the deformation. Equivalently, $\lambda_1^2(F) \leq \lambda_2^2(F) \leq \lambda_3^2(F)$ are the ordered eigenvalues of both Cauchy-Green strain tensors $F^T F$ and $F F^T$. The assumption of incompressibility, which is described by the constraint $\det F = 1$ on deformations with finite energy, corresponds to $\lambda_1 \lambda_2 \lambda_3 = 1$. A global multiplicative factor, often called the rubber energy scale, has been left out in (4) without loss of generality. It is easy to check that $W(F) \geq 0$ for every F, and that $W(F) = 0$ if and only if $F \in \mathcal{K}$.

The energy (4) is not quasiconvex (for definition and details, see, e.g., Dacorogna, 1989; Müller, 1999). This means that it describes a system for which energy minimization may promote the development of fine phase mixtures, as is
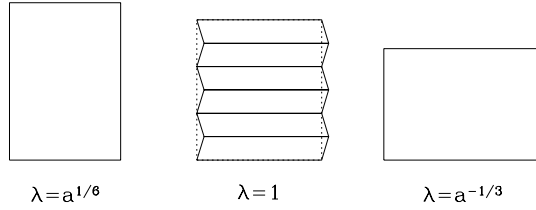
FIGURE 2. Deformation path corresponding to Eq. (5). We plot the shape at $\lambda = a^{1/6}$ (initial state, pure phase), at $\lambda = 1$, and at $\lambda = a^{-1/3}$ (final state, pure phase). The intermediate deformation can be realized through a decomposition into zero-energy stripe-shaped regions, see Eq. (6).

best illustrated heuristically by the following example (see Verwey et al., 1996, for a more detailed discussion). Consider a sheet of nematic elastomer whose mid-surface is orthogonal to $\mathbf{e}_1$, and which is initially in the zero energy configuration described by $F_0 = U_{\mathbf{e}_3}$. Assume now that the sheet is stretched in direction 2 while the F_{11} component is kept fixed, so that the macroscopic deformation gradient of the sheet is

$$(5) \qquad F_t = \begin{pmatrix} a^{1/6} & 0 & 0 \\ 0 & \lambda(t) & 0 \\ 0 & 0 & a^{-1/6}/\lambda(t) \end{pmatrix}$$

with $\lambda(t)$ increasing from $\lambda(0) = a^{1/6}$ to $\lambda(1) = a^{-1/3}$. The final state is the pure state $F_1 = U_{\mathbf{e}_2}$. For $0 < t < 1$ the average deformation F_t is not in $\mathcal{K}$, and the microscopic energy $W(F_t)$ is positive. However, one can find $\delta(t)$ such that

$$(6) \qquad F_t^{\pm} = \begin{pmatrix} a^{1/6} & 0 & 0 \\ 0 & \lambda(t) & \pm\delta(t) \\ 0 & 0 & a^{-1/6}/\lambda(t) \end{pmatrix}$$

belong to $\mathcal{K}$, and satisfy $F_t^+ - F_t^- = 2\delta(t)\mathbf{e}_2 \otimes \mathbf{e}_3$, $F_t^+ + F_t^- = 2F_t$ [in particular, one gets $\delta^2 = (a^{-2/3} - \lambda^2)(1 - a^{1/3}\lambda^{-2})$]. It follows that one can decompose the domain in many stripes (or "layers") of equal thickness and orthogonal to $\mathbf{e}_3$, so that half of the volume is deformed according to F_t^+, the other half according to F_t^-. This realizes an average deformation F_t with zero energy. By making the subdivision finer and finer the displacements converge uniformly to those corresponding to the affine deformation F_t. Of course, many other constructions can be obtained, e.g. using different proportions of the two gradients, or more than two gradients, or interfaces in other directions, see DeSimone and Dolzmann (2000).

The discussion above shows that the value of the microscopic energy density $W(F)$ does not give the actual energetic cost of imposing a given macroscopic deformation F, unless the possibility of energy reduction through the development of fine phase mixtures is correctly taken into account (see, e.g., Ball and James, 1987, 1992, and the references quoted therein for a discussion of this issue in the context

of phase transforming crystalline solids). Explicit resolution of the microscopic oscillations cannot be done with a scale-invariant model such as $W(F)$, within which oscillations may occur at an arbitrarily small length scale (possible regularizations, such as terms with higher order gradients, lead to microstructures with small but finite size, but require much higher computational effort). The effects of fine-scale oscillations can, however, be accounted for by optimizing either numerically or analytically over all possible local microstructures. In the case of nematic elastomers, the high symmetry present in $W(F)$ permits an exact analytical calculation of the resulting effective (or quasiconvexified) energy density.

The quasiconvex envelope of W (for details see Dacorogna, 1989; Müller, 1999, and references therein),

(7)
$$W_{qc}(F) = \inf_{y \in W^{1,\infty}} \left\{ \frac{1}{|\Omega|} \int_\Omega W(\nabla y(x))dx : y(x) = Fx \text{ on } \partial\Omega, \det \nabla y(x) = 1 \right\},$$

coarse-grains the energetics of the system: it gives the minimum energy needed to produce the macroscopic deformation F, optimized over all possible admissible microstructures $y(x)$. Here the notation $y \in W^{1,\infty}$ means that y is Lipschitz-continuous. Note also that the domain Ω, whose volume we denote by $|\Omega|$, plays here the role of a representative volume element: it can be verified that W_{qc} does not depend on Ω. The use of W_{qc} in the numerical computations allows one to resolve only the macroscopic length scale, with the (possibly infinitesimal) microscopic scale already accounted for in W_{qc}. Clearly, this approach gives only average information on the fine phase mixtures and focuses on the macroscopic response of the system.

For nematic elastomers, an explicit formula for W_{qc} has been derived by DeSimone and Dolzmann (2001), which for volume-preserving deformation gradients reads

(8)
$$W_{qc}(F) = \begin{cases} 0 & \text{(phase L) if } \lambda_1 \geq a^{1/6} \\ W(F) & \text{(phase S) if } a^{1/2}\lambda_3^2\lambda_1 > 1 \\ \lambda_1^2 + 2a^{1/2}\lambda_1^{-1} - 3a^{1/3} & \text{(phase Sm) else} \end{cases}$$

while it is infinite if $\det F \neq 1$. Figure 8 represents the phase diagram corresponding to (8), in the $(\lambda_3, \lambda_1^{-1})$ plane. In the following we present a heuristic derivation of (8), together with a discussion of its implications on the mechanical response of nematic elastomers.

The three regimes in (8) arising from the collective behavior of energetically optimal fine phase mixtures represent three different modes of mechanical response corresponding to three different patterns of decomposition of the local average deformation gradient F. All deformations in the "liquid" phase L can be decomposed in (possibly infinitely many) zero-energy regions, in a way similar to that sketched in Figure 2. An arbitrary (average) deformation gradient within the region L of the phase diagram can be obtained with zero energy by iterating twice the construction presented in Eqs. (5-6), so that up to 4 different gradients are used (laminates within laminates, see DeSimone and Dolzmann, 2001). In this region of the phase diagram the energy is flat, and the mechanical response of the material is liquid-like. For macroscopic deformations in the "solid" phase S one of the eigenvalues of FF^T is large, and the director is naturally parallel to the associated eigenvector. Hence the freedom to form microstructure does not allow to reduce the energy, i.e. $W_{qc} = W$, and the mechanical response is that of a solid rubber. Finally, in

the "smectic" region Sm of the phase diagram, the material exhibits a smectic-like response characterized by one small singular value, λ_1, which alone determines the energy. To understand how this happens, consider a deformation gradient with singular values $\lambda_3 \geq \lambda_2 \geq \lambda_1$, such that $\lambda_1 \leq a^{1/6}$. At fixed λ_1, the energy depends on λ_2 and λ_3. The minimum energy is obtained by minimizing $a\lambda_3^2 + \lambda_2^2$ with the constraint $\lambda_2\lambda_3 = 1/\lambda_1$, which gives $\lambda_2^2 = a^{1/2}/\lambda_1$, $\lambda_3^2 = 1/\lambda_1 a^{1/2}$. Consider now the decomposition of the average deformation gradient

$$(9) \qquad F = \begin{pmatrix} \lambda_1 & 0 & 0 \\ 0 & \lambda_2 & 0 \\ 0 & 0 & \lambda_3 \end{pmatrix}$$

into two variants

$$(10) \qquad F_\delta^\pm = \begin{pmatrix} \lambda_1 & 0 & 0 \\ 0 & \lambda_2 & \pm\delta \\ 0 & 0 & \lambda_3 \end{pmatrix} .$$

We seek δ so that the singular values of $F_\delta^\pm$ are the optimal ones at fixed λ_1, i.e. $(\lambda_1, a^{1/4}\lambda_1^{-1/2}, a^{-1/4}\lambda_1^{-1/2})$. Equating the sum of their squares to the trace of $(F_\delta^+)^T F_\delta^+$ we get

$$(11) \qquad \lambda_1^2 + \frac{a^{1/2}}{\lambda_1} + \frac{1}{a^{1/2}\lambda_1} = \lambda_1^2 + \lambda_2^2 + \lambda_3^2 + \delta^2$$

which can be solved for δ provided that $\lambda_2/\lambda_3 + \lambda_3/\lambda_2 \leq a^{1/2} + a^{-1/3}$. Given the ordering condition, this amounts to $\lambda_2/\lambda_3 \leq a^{1/2}$, or equivalently, to $a^{1/2}\lambda_1\lambda_3^2 \geq 1$. If this condition is satisfied, then the energy depends only on λ_1, and computing its value we obtain exactly the result for phase Sm in Eq. (8). The proof of Eq. (8) is then concluded by showing that all the constructions performed above are optimal, in the sense that no other construction can give smaller energy (see DeSimone and Dolzmann, 2001, for the details).

In phase Sm the energy is flat with respect to changes in the two larger eigenvalues, i.e., there exist in-plane strains which cause no elastic reaction (as long as one does not cross the phase boundary). More precisely, given the volume constraint, and going to the plane-stress case of interest here, we see that in phase Sm only the in-plane area enters the energy, whereas in-plane shears are completely soft. The role of this peculiar smectic-like phase will be discussed later. It is however clear that, as long as part of the system is inside regions L or Sm, there will be non-uniqueness not only of the energetically optimal microstructure, but also of the macroscopic deformation gradient. The selection mechanism we introduced to resolve this degeneracy is explained in Section 4.

The implementation of this macroscopic effective energy W_{qc} in a finite-element code is the starting point for our numerical experiments.

3. Numerical simulation of a stretching experiment

In this section we present the results from our computations based on the quasi-convexified energy W_{qc} on a model problem, whose geometry and material parameter have been chosen to agree with typical experiments reported in the literature. Common values for a, typically denoted by $1/r$ or $(l_\perp^0/l_\parallel^0)^2$, are between 0.35 and 0.7 (Finkelmann et al., 1997; Warner and Terentjev, 1996; Zubarev et al., 1999). We take $a = 0.5$, which corresponds to a spontaneous stretch $a^{-1/3} = 1.26$. The
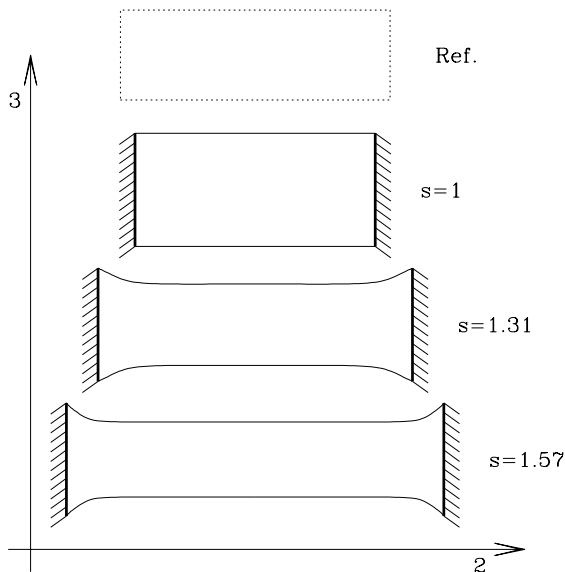
FIGURE 3. Experimental geometry. The top figure (dotted) is the
reference configuration, with aspect ratio 3. The second figure rep-
resents the initial condition, obtained through an affine deforma-
tion with gradient $U_{\mathbf{e}_3}$. We then prescribe uniform displacements
in direction 2 on the two faces with normal $\mathbf{e}_2$ (thicker lines). The
rest of the boundary is free, and the out-of-plane component of the
displacement is free for the entire sample. The remaining figures
will exploit symmetry and display only one quarter of the system.

loading process of the experiments and of our simulations consists in stretching
a thin, flat rectangular sheet in a direction orthogonal to the director at cross-
linking, as illustrated in Figure 3. The reference configuration is the stress-free
configuration in the high temperature phase (this corresponds to $a = 1$), which is
given by a sheet with rectangular mid-surface and aspect ratio $l_2/l_3 = 3$ (we also
performed simulations with $l_2/l_3 = 1$, see below). The thickness of the sheet is
fixed by $l_1 = 0.1l_3$. The initial configuration is the stress-free one (in the low tem-
perature phase, i.e. for $a = 0.5$) with director parallel to $\mathbf{e}_3$, hence it is deformed
with respect to the reference configuration by the affine uniaxial strain $U_{\mathbf{e}_3}$. The
aspect ratio in the initial configuration is thus $3a^{1/2} \sim 2.12$. In the experiment,
the two faces orthogonal to $\mathbf{e}_2$ are glued to two pieces of rigid material (clamps),
which are then pulled away from each other. In our simulation, on those faces we
impose displacement boundary conditions. The stretch s is the distance between
the clamps (in direction 2) in units of its initial value. At the level of the present
analysis the problem is scale-invariant, and only ratios of lengths are meaningful.
We always work with zero tractions on the unclamped part of the boundary. Com-
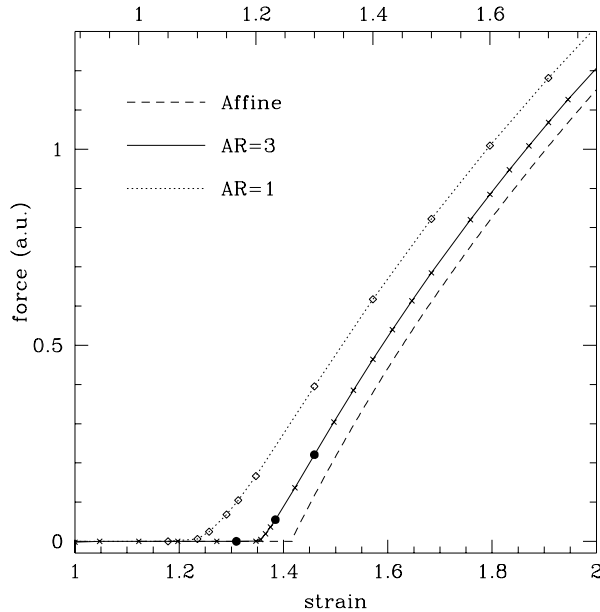putations have been performed by implementing a user-defined constitutive law in

FIGURE 4. Force versus strain curve (crosses joined by the full line). The dashed curve gives the analytic result for affine deformations from Eq. (12). The diamonds joined by the dotted curve are results obtained for aspect-ratio 1. The three black dots mark the configurations which are presented in more detail in the following figures. The top axis gives the strain with respect to the reference configuration, namely, $sa^{1/6}$.

the finite-element software package ABAQUS on a SUN workstation. We describe details of the numerical procedure in Section 4.

Figure 4 shows the reactive force exerted by the clamps plotted against the imposed displacements. For comparison we also plot the corresponding graph resulting from the affine approximation, on which most previous theoretical analyses are based. The affine approximation amounts to neglecting the constraint exerted by the clamps against contractions in direction 3, and it gives

$$(12) \qquad f_{\text{affine}}(s) = \begin{cases} 0 & \text{if } 1 \leq s \leq a^{-1/2} \\ 2a^{4/3}s - 2a^{-1/6}s^{-2} & \text{if } s > a^{-1/2}. \end{cases}$$

It is clear from Figure 4 that the existence of a "window" of liquid-like behavior, where the force is identically zero, is correctly predicted by the affine approximation, but its width is overestimated, especially for the smaller aspect ratio. This trend is easily understood considering that contractions in direction 3 are hindered only in the regions around the clamps, whereas the central part of the sample is in all cases deformed almost affinely. The force in the liquid window $(1 \leq s \leq 1.35)$ is zero within our numerical precision (see Section 4).

The transition between a liquid-like mode of response, in which no force is transmitted in the longitudinal direction, and a solid-like one, in which the clamps exert

FIGURE 5. Density plot of the von Mises stress at stretch $s = 1.38$.
For greater clarity, the full sample is displayed here (computations
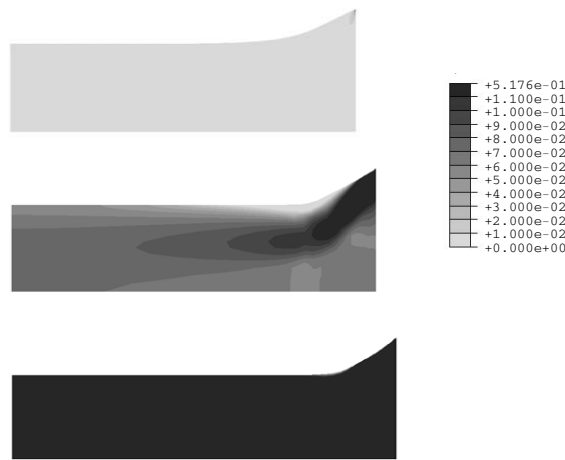have been performed on one quarter only).

FIGURE 6. Density plot of the von Mises stress at stretches 1.31
(top), 1.38 (center) and 1.46 (bottom). The central figure is the
same as in Figure 5.

non-zero force, is also evident from the plot of the von Mises stress in Figures 5 and
6. It is clear from the data at $s = 1.38$ that the upper-right corner is particularly
stressed (and, changing scale, this remains true at all values of s we studied). Fur-
ther, we observe that stresses are transmitted along an X-shaped path connecting
the center of the sample to the end points of the clamps. The stress transmission
path develops some characteristic kinks near the clamps (the origin of these kinks
is further discussed below), and it leaves some regions (the parts close to the center
of the clamped boundary and the parts near the sharp angle in the free boundary)
relatively unstressed.

The low-stress sharp angle in the free boundary is indeed a peculiar feature of the
material under study. In Figure 7 we compare the profiles we obtained with those
of a standard neo-Hookean material [obtained by setting $a = 1$ in the expression
for $W(F)$]. Even though the configurations at small stretches may be affected
by our regularization procedure (see Section 4), the data seem to suggest that the
curvature of the free edge is consistently much more localized in nematic elastomers
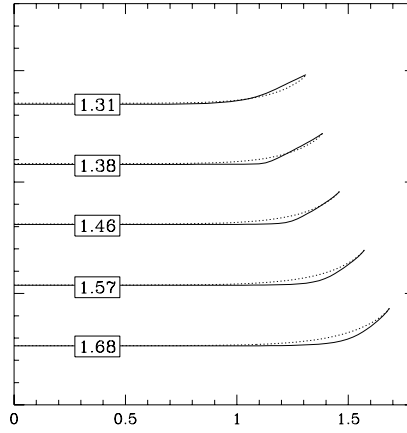than in more conventional rubbers.

FIGURE 7. Sample profile (full curves) at various stretches, compared with the corresponding result for a neo-Hookean material (dotted curves).
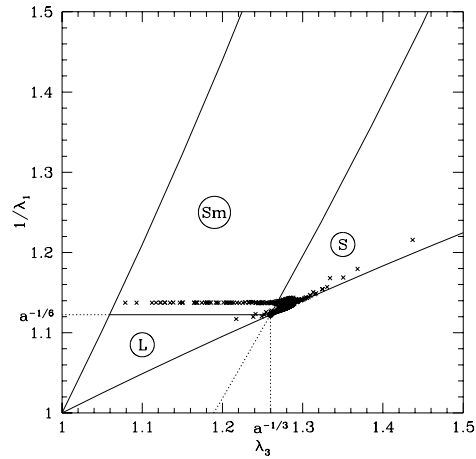

FIGURE 8. Mesoscopic phase diagram and phase distribution at $s = 1.38$. The three regions are defined in Eq. (8). Only the region $\lambda_3^2 \geq 1/\lambda_1 \geq \lambda_3^{1/2}$ can be attained (due to the volume constraint).

To obtain a more detailed understanding of the microscopic mechanisms that determine the macroscopic response in our system, we need to analyze in detail the role of the three different phases L, S, and Sm, corresponding to the three different expressions for the energy W_{qc} in Eq. (8). Figure 8 shows the points in the mesoscopic phase diagram which are used in the macroscopic deformation computed for $s = 1.38$. In phase Sm, the energy only depends on the smallest
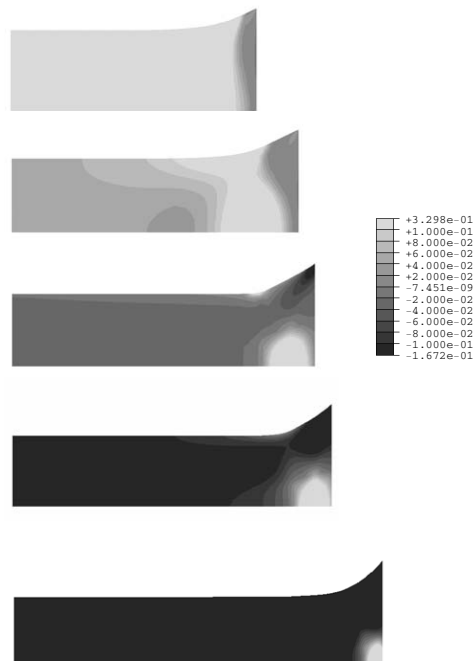
FIGURE 9. Plot of the microstructure index I_M for different stretches. From top to bottom, $s = 1.12$, $s = 1.31$, $s = 1.38$, $s = 1.46$, and $s = 1.68$.

eigenvalue λ_1 [see Eq. (8)]. The row of points in phase Sm at $\lambda_1 =$ constant corresponds to elements which are in-plane expanded, hence compressed in the thickness direction due to the volume constraint. The location of these points within the sample explains the kinks in the stress transmission paths, as discussed below. The in-plane shears within phase Sm can be instead all accommodated at no energy cost with the mechanism outlined in Section 2.

In several experiments (Kundler and Finkelmann, 1995; Zubarev et al., 1999) formation of domains in the shape of narrow stripes has been observed in the central part of the sample. This is explained by the fact that, in this region, the energy is reduced by forming small-scale oscillatory patterns with alternating shears. As explained in Section 2, however, this can happen for averaged deformation gradients both in phase L and in phase Sm. To verify which points are in these two regions, we plot the microstructure index

$$(13) \qquad\qquad I_M = \frac{1}{\lambda_1} - a^{1/2}\lambda_3^2$$

which is positive in phases L and Sm, and negative in phase S. Hence, $I_M > 0$ characterizes regions where the macroscopic deformation is achieved by a mixture of different microscopic deformations. Figure 9 shows a density plot of I_M for different stretches. The striking result is that microstructures remain present even at large stretches, near the mid-point of the clamped edge. By comparing the plots of I_M with those of the von Mises stress, Figure 6, one can see that at large stretches this region is not stress-free. Thus, it must be composed of average deformation
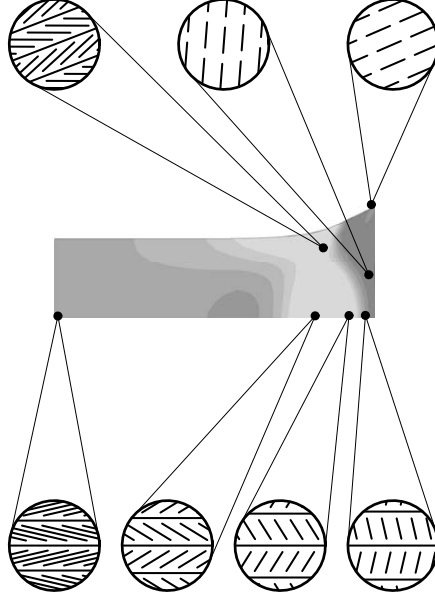
FIGURE 10. Microstructure index I_M and resolution in microstructures at stretch 1.31. Scale as in Fig. 9.

gradients in phase Sm, i.e., of stressed fine phase mixtures whose energy depends essentially only on the in-plane change of area. With increasing stretch, the regions containing microstructure migrate towards the clamped ends of the sample. Here, due to the presence of the clamps, the local stretch in the x_2 direction is lower than the imposed average stretch s.

From an intuitive point of view, the existence of an "island" exhibiting microstructure near the clamped ends can be understood as follows. Since the rigid clamps do not allow contractions along direction 3, for the material near the clamped ends the maximum stretch is along direction 3, at least for moderate values of s. The central part of the sample (left side of Fig. 9) is instead free to relax in direction 3, and it reacts to the imposed elongation in direction 2 by contracting along direction 3. It follows that, along the mid-axis of the sample (the lower side in the figure) the two in-plane stretches have to change their ordering: the point where they are equal ($\lambda_3 = \lambda_2 = \lambda_1^{-2}$) lies in phase Sm. Since these stressed microstructures transmit in-plane tractions (with equal principal stresses), they "pull" the stress transmission path towards the center of the clamped edge. This explains the sharp kinks in the stress transmission path of Figure 5. We also note that, since these stressed phase mixtures entail higher compressive strains in the thickness direction, the existence of regions with smectic microstructure near the clamps should be amenable to experimental verification.

Further understanding of the microscopic mechanisms responsible for the observed macroscopic behavior can be achieved by reconstructing one possible realization of the composite structures of phases L and Sm. In spite of the non-uniqueness associated with this process (see discussion below), it is instructive to
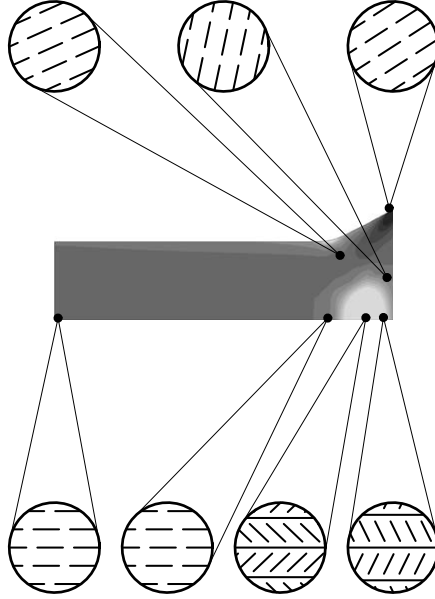
FIGURE 11. Microstructure index I_M and resolution in microstructures at stretch 1.38. Scale as in Fig. 9.
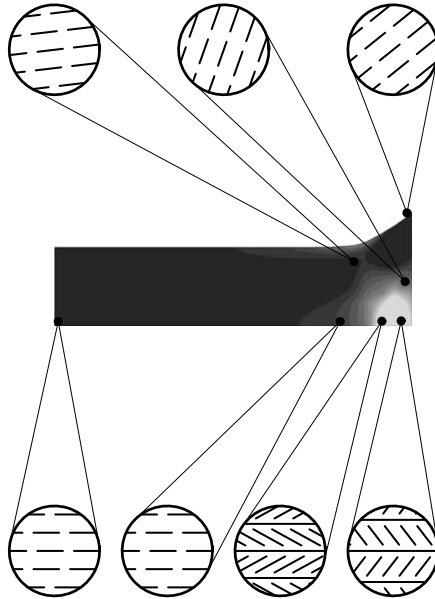

FIGURE 12. Microstructure index I_M and resolution in microstructures at stretch 1.46. Scale as in Fig. 9.

consider the blow-ups in Figures 10, 11, and 12 as suggestions of the possible geometry of the microstructure in those regions. They have been obtained with a

decomposition procedure analogous to the one of Eqs. (9-10) from the computed deformation gradients. The "sticks" in the figures indicate the local orientation of the nematic director $\mathbf{n}$, and have been obtained by plotting the eigenvector of FF^T corresponding to its largest eigenvalue λ_3^2.

The results of our computations are fully consistent with the experimental observation of stripes parallel to direction 2 by Kundler and Finkelmann (1995), and with the spatially inhomogeneous microstructures reported by Zubarev et al. (1999).

4. SELECTION MECHANISM AND COMPUTATIONAL ISSUES

Our computations have been performed on one-eighth of the physical domain (exploiting symmetry), with a rectangular grid with 800 volume-constrained 8-node elements, with a non-uniform mesh refining towards the edges of the clamp (see Fig. 13), and using a reverse loading path. The energy was W_{qc} plus a small constant μ times a neo-Hookean perturbation [see Eq. (14)]. In the rest of this section we briefly discuss the technical aspects of the computations we presented, and we explain our computational strategy. Since the only non-standard part is the use of a neo-Hookean regularizing perturbation as selection mechanism to break the degeneracy associated with W_{qc}, we focus our discussion on this point.

The main difficulty in performing finite-element computations with the quasi-convexified energy W_{qc} is the existence of multiple minima, which directly follows from the existence of flat regions in the graph of $W_{qc}(F)$ (phases L and Sm). This problem is particularly relevant at small stretches, where phase L dominates the picture: W_{qc} is identically zero and it does not provide much information about the actual configuration of the system. We chose one among all degenerate states by using a small neo-Hookean perturbation as the selection mechanism, i.e., by replacing W_{qc} with

$$(14) \qquad W_{\mathrm{reg}}(F) = W_{\mathrm{qc}}(F) + \frac{1}{2}\mu(\mathrm{Tr}F^T F - 3)\,.$$

The expression $\mathrm{Tr}F^T F - 3$, where Tr denotes the trace, corresponds to $W(F)$ taken at $a = 1$, hence it can be seen as the energy of the parent isotropic phase. Suitably tuning the value of the parameter μ, which represents the shear modulus at $F = \mathrm{Id}_3$, allowed us to continuously change from a numerically very stable system (μ of order 1, which is the energy scale of W_{qc}) to a very accurate representation of the real system (μ small). In practice, we took the system to the desired value of average stretch s with $\mu = 10^{-2}$, and then relaxed the system to $\mu = 10^{-4}$ while keeping the stretch fixed. Observing the change of the deformation during this relaxation process we checked that the dependence of the results on the actual value of μ was small.

The rationale behind the choice of this selection mechanism is to replace the search for the non-unique minimum of W_{qc} with the search for the limit, for $\mu \to 0$, of the minimum of W_{reg}. A deeper understanding of the influence of the choice of a regularizing perturbation (which could be designed to capture the deviations of the actual physical system from the ideally soft behavior, or which, less ambitiously, could simply amount to imposing additional conditions on the energy minimizers) would certainly be desirable, but is beyond the scope of the present study.

We now come to the dependence of the results on the value of μ. The transmitted force is the quantity we chose to obtain a quantitative estimate of how much our
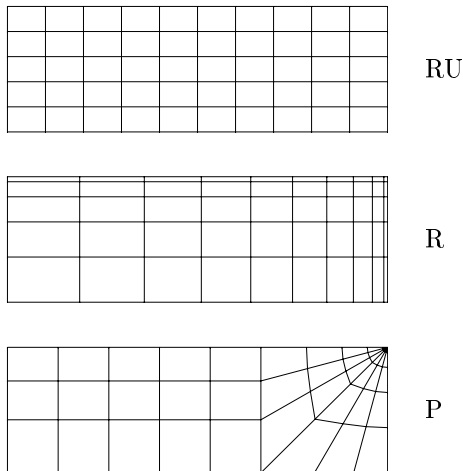
FIGURE 13. Different types of grids, in the reference configuration. RU denotes rectangular uniform (i.e., node positions scale linearly with node index); R denotes non-uniform rectangular (i.e., node positions scale quadratically with node index); P denotes polar (i.e., a square at the clamped end is covered by a polar grid centered on the upper right corner). Our results have been obtained with a grid of type R with 40 elements in the horizontal direction, 20 in the vertical one, and one along the thickness.

results are affected by the neo-Hookean perturbation. In Figure 14 we plot the dependence of the force at $s = 1.38$ on μ, together with a linear two-parameter fit

$$(15) \qquad\qquad f(\mu) = f(0) + \mu g \,.$$

The good quality of the fit, and the small residual dependence for $\mu \leq 10^{-4}$, allow one to safely take the extrapolated value as the value which corresponds to the $\mu \to 0$ limit. All values presented in Figure 4 have been obtained performing such a fit. For quantities different from the force, the quality of the results at $\mu = 10^{-4}$ was judged to be satisfactory, and no extrapolation was needed.

We found that computational efficiency could be significantly increased by simulating the reverse experiment, i.e. preparing the system in a pre-stretched ($s \sim 2$) state with $\mu = 1$, then reducing μ to 10^{-2}, and finally reducing s. This amounts to performing first the more stable part of the simulation, which increases both stability and speed. We verified in some representative cases that the state we reached did not depend on the path followed in the (s, μ) plane.

We performed computations both with a rectangular grid and with a polar one, with origin in the upper-right corner of the sample (see Fig. 13). We found no significant differences when simulating with one, two, or four elements in the thickness direction. Similarly, simulations with smaller thickness lead to essentially the same results (except for the obvious scaling of the total force with the sample cross-section). In the case of the rectangular grid we tested both uniform grids and grids with node positions scaling quadratically with node index. We tested different types of volume-constrained elements (C3D8H, C3D20H, and C3D8RH
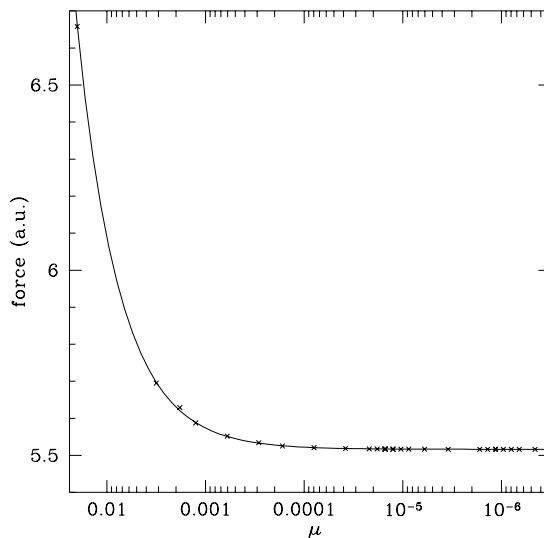
FIGURE 14. Transmitted force at $s = 1.38$ for various values of the regularization parameter μ (crosses), and fit according to Eq. (15) (full curve). The straight line of Eq. (15) becomes an exponential on a semilogarithmic scale.

of Abaqus, 1998), and always found very similar results. The results presented here have been obtained with the rectangular non-uniform grid with 8-node linear elements, which allowed us to obtain the same quality with fewer elements (and hence smaller computational cost) than the others.

5. SUMMARY AND CONCLUDING REMARKS

We have studied numerically the mechanical response of stretched nematic elastomers, observing qualitative agreement with available experiments. From a methodological point of view, we have shown with an experimentally relevant case study how knowledge of the quasiconvex envelope of a microscopic energy allows one to perform finite-element computations of phase-transforming materials exhibiting microstructure. We have discussed the new difficulties with which one is faced, mainly due to the degeneracy of the quasiconvex envelope, and have shown how they can be overcome, at least in this example.

From the point of view of the physics of nematic elastomers, we have discovered a new, smectic-like mode of response of the system arising from microscopic mixtures of stressed states, and we have highlighted its role in determining the stress transmission paths in stretched sheets. Moreover, we have shown that the existence of a window of liquid-like response is compatible with the spatial non-uniformity of the stretches induced by rigid clamps, although its width is progressively reduced with respect to the affine approximation as the aspect ratio of the sample decreases. We have also shown that regions with fine phase mixtures survive even at high strains, in pockets near the midpoints of the clamps. These regions, however, are mapped to points located in the smectic-like part of the phase diagram of W_{qc}. Thus, they

do not transmit in-plane shears, but they do transmit in-plane tractions which are the elastic reactions to local changes of area, and these tractions explain the shape of the stress transmission paths.

Our results show good qualitative agreement with the available experimental results, and provide quantitative theoretical predictions on the force and on the geometry of the deformed sample, some of which are amenable to experimental validation.

Many relevant questions are still open on this fascinating system: in particular, those related to the degeneracy of the response of an ideally soft system. At a mathematical level, a deeper understanding of the non-uniqueness of energy minimizing configurations would be desirable. At the modeling level, the natural next step seems to investigate stress inhomogeneity starting from a microscopic energy capable of capturing the observed deviations from the ideally soft behavior.

REFERENCES

Abaqus, 1998. Abaqus/Standard User's Manual, version 5.8. Hibbitt, Karlsson and Sorensen Inc.

Ball, J. M., James, R. D., 1987. Fine phase mixtures as minimizers of energy. Arch. Rat. Mech. Anal. 100, 13–52.

Ball, J. M., James, R. D., 1992. Proposed experimental tests of a theory of fine microstructure and the two-well problem. Phil. Trans. R. Soc. Lond. A 338, 389–450.

Bladon, P., Terentjev, E. M., Warner, M., 1993. Transitions and instabilities in liquid-crystal elastomers. Phys. Rev. E 47, R3838–R3840.

Dacorogna, B., 1989. Direct methods in the calculus of variations. Springer.

DeSimone, A., 1999. Energetics of fine domain structures. Ferroelectrics 222, 275–284.

DeSimone, A., Dolzmann, G., 2000. Material instabilities in nematic elastomers. Physica D 136, 175–191.

DeSimone, A., Dolzmann, G., 2001. Macroscopic response of nematic elastomers via relaxation of a class of SO(3)-invariant energies, in preparation.

Finkelmann, H., Kundler, I., Terentjev, E. M., Warner, M., 1997. Critical stripe-domain instability of nematic elastomers. J. Phys. II France 7, 1059–1069.

Golubović, L., Lubensky, T. C., 1989. Nonlinear elasticity of amorphous solids. Phys. Rev. Lett. 63, 1082–1085.

Kundler, J., Finkelmann, H., 1995. Strain-induced director reorientation in nematic liquid single crystal elastomers. Macromol. Rapid Comm. 16, 679–686.

Müller, S., 1999. Variational models for microstructure and phase transitions. In: Bethuel, F., Huisken, G., Müller, S., Steffen, K., Hildebrandt, S., Struwe, M. (Eds.), Calculus of Variations and Geometric Evolution Problems, Lectures given at the 2nd Session of the Centro Internazionale Matematico Estivo, Cetraro 1996. Springer, Berlin.

Verwey, G. C., Warner, M., Terentjev, E. M., 1996. Elastic instability and stripe domains in liquid crystalline elastomers. J. Phys. II France 6, 1273–1290.

Warner, M., 1999. New elastic behaviour arising from the unusual constitutive relation of nematic solids. J. Mech. Phys. Sol. 47, 1355–1377.

Warner, M., Terentjev, E. M., 1996. Nematic elastomers - a new state of matter? Prog. Polym. Sci. 21, 853–891.

Weilepp, J., Brand, H. R., 1996. Director reorientation in nematic-liquid-single-crystal elastomers by external mechanical stress. Europhys. Lett. 34, 495–500.

Zubarev, E. R., Kuptsov, S. A., Yuranova, T. I., Talroze, R. V., Finkelmann, H., 1999. Monodomain liquid crystalline networks: reorientation mechanism from uniform to stripe domains. Liquid Crystals 26, 1531–1540.

SERGIO CONTI, MAX PLANCK INSTITUTE FOR MATHEMATICS IN THE SCIENCES, INSELSTR. 22-26, D-04103 LEIPZIG, GERMANY

E-mail address: conti@mis.mpg.de

ANTONIO DESIMONE, MAX PLANCK INSTITUTE FOR MATHEMATICS IN THE SCIENCES, INSELSTR. 22-26, D-04103 LEIPZIG, GERMANY, AND DIPARTIMENTO DI INGEGNERIA CIVILE E AMBIENTALE, POLITECNICO DI BARI, I-70126 BARI, ITALY

E-mail address: desimone@mis.mpg.de

GEORG DOLZMANN, MATHEMATICS DEPARTMENT, UNIVERSITY OF MARYLAND, COLLEGE PARK, MD 20742, U.S.A.

E-mail address: dolzmann@math.umd.edu